PHYSICAL REVIEW APPLIED **1,** 051002 (2014)

Orientational Tuning of the Fermi Sea of Confined Electrons at the $SrTiO_3$ (110) and (111) Surfaces

T. C. Rödel,[1,2] C. Bareille,[1] F. Fortuna,[1] C. Baumier,[1] F. Bertran,[2] P. Le Fèvre,[2] M. Gabay,[3] O. Hijano Cubelos,[3] M. J. Rozenberg,[3,4] T. Maroutian,[5] P. Lecoeur,[5] and A. F. Santander-Syro[1,*]

[1]*CSNSM, Université Paris-Sud and CNRS/IN2P3, Bâtiments 104 et 108, 91405 Orsay cedex, France*
[2]*Synchrotron SOLEIL, L'Orme des Merisiers, Saint-Aubin-BP48, 91192 Gif-sur-Yvette, France*
[3]*Laboratoire de Physique des Solides, Université Paris-Sud and CNRS, Bâtiment 510, 91405 Orsay, France*
[4]*Departamento de Física–IFIBA Conicet, FCEN, UBA, Ciudad Universitaria P.1, 1428, Buenos Aires, Argentina*
[5]*Institut d'Electronique Fondamentale, Université Paris-Sud and CNRS, Bâtiment 220, 91405 Orsay, France*

(Received 1 March 2014; revised manuscript received 17 May 2014; published 18 June 2014)

We report the existence of confined electronic states at the (110) and (111) surfaces of $SrTiO_3$. Using angle-resolved photoemission spectroscopy, we find that the corresponding Fermi surfaces, subband masses, and orbital ordering are different from the ones at the (001) surface of $SrTiO_3$. This occurs because the crystallographic symmetries of the surface and subsurface planes and the effective electron masses along the confinement direction influence the symmetry of the electronic structure and the orbital ordering of the t_{2g} manifold. Remarkably, our analysis of the data also reveals that the carrier concentration and thickness are similar for all three surface orientations, despite their different polarities. The orientational tuning of the microscopic properties of two-dimensional electron states at the surface of $SrTiO_3$ echoes the tailoring of macroscopic (e.g., transport) properties reported recently in $LaAlO_3/SrTiO_3$ (110) and (111) interfaces, and is promising for searching new types of two-dimensional electronic states in correlated-electron oxides.

DOI: 10.1103/PhysRevApplied.1.051002

Two-dimensional electron gases (2DEGs) in transition-metal oxides (TMOs) present remarkable phenomena that make them unique from a fundamental viewpoint and promising for applications [1,2]. For instance, heterostructures grown on the (001) surface of $SrTiO_3$, a TMO insulator with a large band gap of approximately 3.5 eV, can develop 2DEGs showing metal-to-insulator transitions [3], superconductivity [4], or magnetism [5,6]. Recently, 2DEGs at the (111) and (110) interfaces of $LaAlO_3/SrTiO_3$ were also reported [7]. The latter showed a highly anisotropic conductivity [8] and a superconducting state spatially more extended than the one at the (001) interface [9]. Interestingly, theoretical works have also predicted that exotic, possibly topological, electronic states might occur at interfaces composed of (111) bilayers of cubic TMOs [10–13], as two (111) planes of transition-metal ions form a honeycomb lattice, similar to the one found in graphene. In this context, the discoveries that 2DEGs can also be created at the bare (001) surfaces of $SrTiO_3$ [14–16] and $KTaO_3$ [17,18], and more recently at the (111) surface of $KTaO_3$ [19], open new roads in the fabrication and study of different types of 2DEGs in TMOs—in particular, using surface-sensitive spectroscopic techniques, which give direct information about the Fermi surface and subband structure of the confined states. The origin of the confinement is attributed to a local doping of the surface region due to oxygen vacancies and/or lattice distortions.

Here we show that new types of 2DEGs can be directly tailored at the bare (110) and (111) surfaces of $SrTiO_3$. Imaging their electronic structure via angle-resolved photoemission spectroscopy (ARPES), we find that their Fermi surfaces, subband masses, and orbital ordering are different from the ones of the 2DEG at the $SrTiO_3(001)$ surface [14,15] and the ones predicted for the bulk, being thus uniquely sensitive to the confining crystallographic direction. This occurs because the crystallographic symmetries of the 2DEG plane, and the effective electron masses along the confinement direction, influence the symmetry of the electronic structure and the orbital ordering of the t_{2g} orbitals. Furthermore, the observed carrier concentrations and 2DEG thicknesses for different surfaces allow us to showcase the impact of oxygen vacancies and of the polar discontinuity on distinctive features of the confined conducting sheet.

The confined states are either created by fracturing the samples in vacuum or by chemically and thermally preparing the surfaces *in situ*, and studied through ARPES at the Synchrotron Radiation Center (SRC, University of Wisconsin, Madison) and the Synchrotron Soleil (France). The sample preparation, similar to that used in Refs. [20,21], is detailed in the Supplemental Material [22]. All through this Letter, we describe the crystal structure in a cubic basis of unit-cell vectors, and note as $[hkl]$ the crystallographic directions in real space, $\langle hkl \rangle$

*andres.santander@csnsm.in2p3.fr

the corresponding directions in reciprocal space, and (hkl) the planes orthogonal to those directions.

The major difference between the confined states at various surface orientations of $SrTiO_3$ originates from the different symmetries of the corresponding crystal planes: fourfold for the (001) plane, twofold for the (110) surface, and sixfold for the (111) surface. Another difference is the polar character of the surface. Thus, while the (001) terminations, namely SrO or TiO_2, are nominally nonpolar, the (110) terminations are alternatively $(SrTiO)^{4+}$ and $(O_2)^{4-}$, and the (111) terminations are either Ti^{4+} or $(SrO_3)^{4-}$. These different surface symmetries and their polarity are illustrated in Figs. 1(a)–1(d). Note, in particular, from Fig. 1(d), that a (111)-type bilayer of Ti^{4+} cations forms a honeycomb lattice, as noted in Ref. [10].

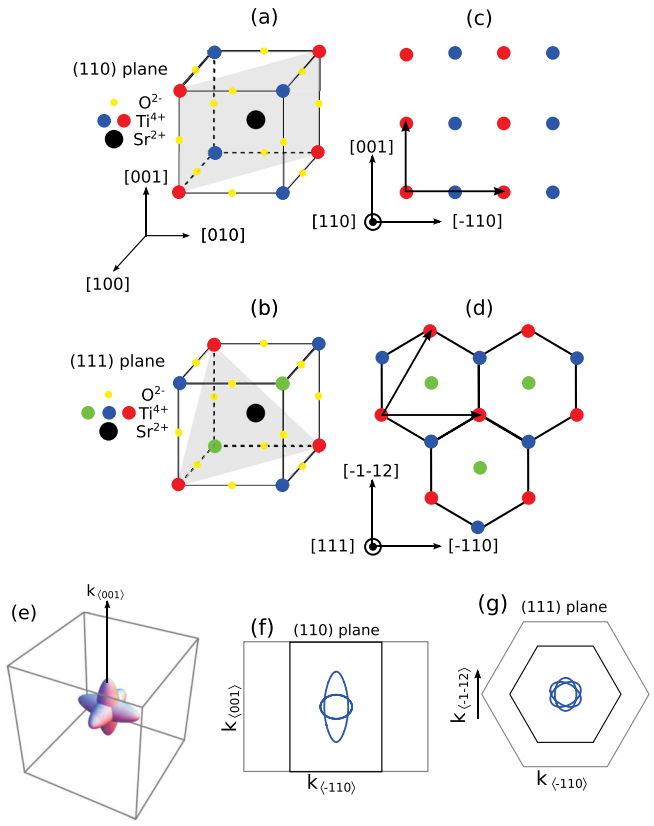

FIG. 1. (a),(b) Unit cell of the cubic perovskite lattice of $SrTiO_3$. The gray planes are the (110) and (111) planes, respectively. The yellow dots represent the O^{2-} anions, the black dot in the center the Sr^{2+} cation, and the red, green, and blue dots the Ti^{4+} cations in different (110) or (111) planes. Both orientations are highly polar, as the crystal is built of alternating layers of $(SrTiO)^{4+}$ and $(O_2)^{4-}$ or Ti^{4+} and $(SrO_3)^{4-}$. (c),(d) Ti^{4+} cations of the crystal lattice at the (110) and (111) planes. The black arrows indicate the lattice vectors of the Ti^{4+} cations in one (110) or (111) plane. As indicated by the black lines in panel (d), a (111) bilayer of Ti^{4+} cations forms a honeycomb lattice. (e) Bulk Fermi surface, calculated using a tight-binding model with an unrealistically large value of 10^{21} cm^{-3} for the bulk carrier density, intended to make the Fermi surface visible. Such a carrier density is at least *3 orders of magnitude* higher than the bulk carrier density of the samples prepared for this study. (f),(g) Cross section of the bulk Fermi surface in (e) along the (110) and (111) planes, respectively. The gray lines show the cross section of the bulk 3D Brillouin zone through a Γ point, while the black lines correspond to the surface Brillouin zone.

For our discussion later, it will be instructive to contrast the observations at the (110) and (111) $SrTiO_3$ surfaces with both the 2DEG at the (001) surface and a model bulk electronic structure. Figure 1(e) shows the bulk Fermi surface from a simplified tight-binding (TB) model where the electron hopping amplitudes between the three t_{2g} orbitals of neighboring Ti^{4+} are $t_\pi = 0.236$ eV and $t_{\delta'} = 0.035$ eV [23], and we neglect spin-orbit coupling and tetragonal distortions. Near the Γ point, this gives effective masses listed in the first row of Table I for various directions. Figures 1(f) and 1(g) show cross sections of the bulk Fermi surface along the (110) and (111) planes through the Γ point, illustrating their respective twofold and sixfold symmetries. The *experimental* spectra at the $SrTiO_3$(001) surface [14], on the other hand, fit well to a TB form where the hopping amplitudes are $\bar{t}_\pi = 0.36$ eV and $\bar{t}_{\delta'} = 0.025$ eV, leading to values of the effective masses near the Γ point shown in the second rows of Table I. Note that all these masses differ by about 30% from the bulk theoretical ones.

We now present our experimental results. Figure 2(a) shows the Fermi surface measured at the *fractured* (110) surface of an undoped *insulating* $SrTiO_3$ sample. As we will see, our observations are similar to another recent study of the 2DEG at the $SrTiO_3$(110) surface in a Nb-doped sample prepared *in situ* by Wang *et al.* [24]. The metallic states we observe present the same twofold symmetry of the unreconstructed (110) surface Brillouin zone, represented by red rectangles. This implies that (i) the macroscopic properties of this 2DEG should be highly anisotropic, echoing the observed anisotropic transport characteristics reported in 2DEGs at (110) $LaAlO_3/SrTiO_3$ interfaces [8], and (ii) any

TABLE I. Effective light (L) and heavy (H) masses predicted by a TB model in the bulk (first row) and experimental in-plane masses of the 2DEGs at the (001), (110), and (111) surfaces (other rows) along the different high-symmetry directions of the crystal lattice (columns) of $SrTiO_3$. In the bulk, all the effective masses along ⟨111⟩ are identical.

	m_{100}/m_e		m_{110}/m_e		$m_{11\bar{2}}/m_e$		m_{111}/m_e
	L	H	L	H	L	H	
Theory bulk[a]	1.06	7.16	1.06	1.85	1.24	2.46	1.48
$SrTiO_3$(001)	0.7[b]	10.0[b]	0.7[c]	1.3[c]	0.8[c]	1.8[c]	1.0[c]
$SrTiO_3$(110)	1.0	8.5	1.6	6.0	···	···	···
$SrTiO_3$(111)	···	···	0.27	1.08	0.33	8.67	···

[a]From Ref. [23].
[b]From Ref. [14].
[c]From the TB model using experimental masses along ⟨100⟩.

surface roughness or reconstructions, expected in this highly polar surface, do not affect the 2DEG, which must then reside in the subsurface layers—in agreement with our previous conclusions on fractured (111) surfaces of $KTaO_3$ [19]. Figure 2(b) shows the dispersion along the $k_{\langle 001\rangle}$ direction, giving rise to the longest of the two ellipsoidal Fermi surfaces in Fig. 2(a). The band forming the shortest ellipsoid is eclipsed by photoemission selection rules along this direction (see the Supplemental Material [22]). The band bottom and Fermi momenta are about −40 meV and 0.3 $Å^{-1}$, respectively.

From the data above, we model the Fermi surface of the 2DEG at the $SrTiO_3(110)$ surface as two orthogonal ellipses, one along $\langle 001\rangle$ with semiaxes of 0.3 and 0.1 $Å^{-1}$, the other along $\langle 1\bar{1}0\rangle$ with semiaxes 0.25 and 0.13 $Å^{-1}$. From the area A_F enclosed by the Fermi surfaces, we obtain a carrier density $n_{2D}^{(110)} = A_F/2\pi^2 \approx 1\times10^{14}$ cm^{-2}. The electronic states associated with such a high charge carrier density must be confined to the region near the surface—otherwise the bulk would be highly conductive, in contradiction with the insulating nature of the samples studied. Similarly, from the band bottom and Fermi momenta, using a parabolic approximation, we obtain the effective band masses along $\langle 001\rangle$ and $\langle \bar{1}\,\bar{1}\,0\rangle$ (and equivalent directions), listed in the third row of Table I. These effective masses are similar to the ones determined in the aforementioned study [24] of the 2DEG at the $SrTiO_3(110)$ surface. In our study, the band bottom of the heavy band, cf. Fig. 2(b), and the carrier density of the 2DEG are slightly lower, probably due to the different surface preparation techniques.

Henceforth, we focus on new experimental results at the (111) surface of $SrTiO_3$, which, as we will see, presents the hexagonal symmetry of the unreconstructed surface, and could thus be an interesting platform for the quest of new electronic states and macroscopic properties at oxide surfaces.

Figure 3(a) shows the Fermi surface measured at the $SrTiO_3(111)$ surface prepared *in situ*, as described in the Supplemental Material [22]. It consists of three ellipses forming a six-pointed star, thus strongly differing from the Fermi surface at the $SrTiO_3(110)$ surface, shown in Fig. 2(a), or the one at the $SrTiO_3(001)$ surface, discussed in previous works [14–16]. Additional experiments show that for surfaces prepared *in situ* with either (1×1) or (3×3) reconstructions, the band structure and periodicity of the confined states are *identical*, and correspond to the one expected from an *unreconstructed surface* [22]. This indicates that the 2DEG at the $SrTiO_3(111)$ surface is also located in the subsurface layers, and is at best weakly affected by the surface reconstructions at the polar (111) surface.

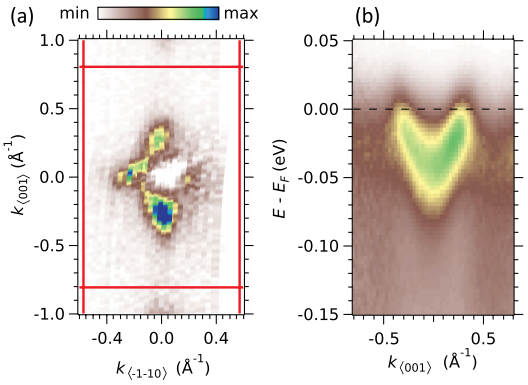

FIG. 2. (a) ARPES Fermi surface map (second derivative) at $h\nu = 91$ eV in the (110) plane of a fractured insulating $SrTiO_3$ sample. The map is a superposition of intensities measured in the bulk Γ_{130} and Γ_{131} Brillouin zones [22]. The red lines indicate the edges of the unreconstructed (110) Brillouin zones. (b) Energy-momentum intensity map at a Γ point along the $k_{\langle 001\rangle}$ direction.

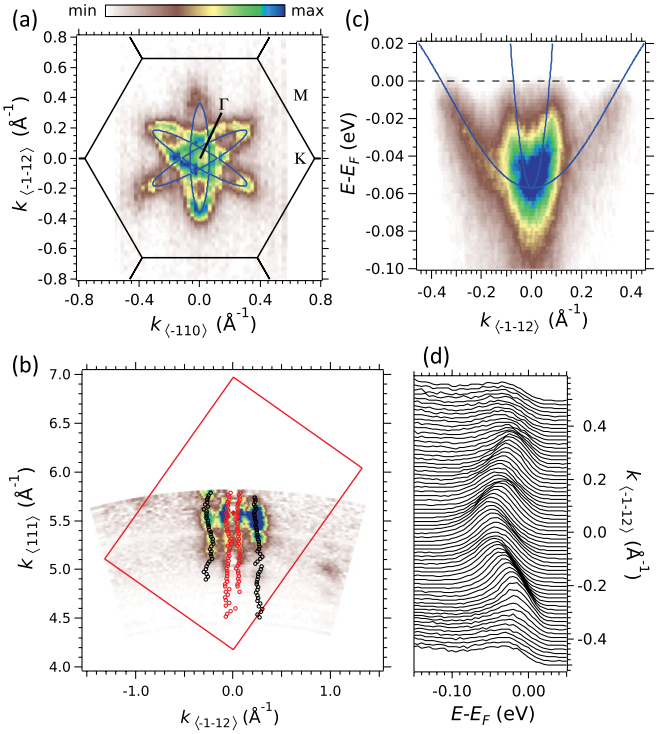

FIG. 3. (a) Fermi surface map measured at $h\nu = 110$ eV on a $SrTiO_3(111)$ surface prepared *in situ*. The black lines indicate the edges of the unreconstructed (111) Brillouin zones around Γ_{222}. (b) Fermi surface map (second derivative of ARPES intensity, negative values) in the $k_{\langle 111\rangle}$-$k_{\langle \bar{1}\,\bar{1}\,2\rangle}$, or $(1\bar{1}0)$ plane, acquired by measuring at normal emission while varying the photon energy in 1 eV steps between $h\nu_1 = 67$ eV and $h\nu_2 = 120$ eV. The experimental Fermi momenta, represented by the black and red circles, are obtained by fitting the momentum distribution curves (MDCs) integrated over $E_F \pm 5$ meV. The red rectangle is the bulk Brillouin zone in the $(1\bar{1}0)$ plane. (c) Energy-momentum map across the Γ point along the $\langle \bar{1}\,\bar{1}\,2\rangle$ direction. The dispersions of a heavy band and light bands are visible. (d) Raw energy distribution curves of the dispersions are shown in panel (c). In panels (a) and (c), the blue lines are simultaneous TB fits to the Fermi surface and dispersions.

The 2D-like character of the electronic states is strictly demonstrated from the Fermi surface map in the $\langle 111\rangle$-$\langle \bar{1}\,\bar{1}\,2\rangle$ plane, shown in Fig. 3(b). Here, one sees that the bands do not disperse along $k_{\langle 111\rangle}$ over more than half a bulk Brillouin zone, thereby confirming the confined (i.e., localized) character of the electrons along the [111] direction in real space. The modulation of the intensity in the Fermi surface map, a typical feature of quantum-well states [25,26], is discussed in the Supplemental Material [22]. Interestingly, note that the red rectangles in Figs. 2(a) and 3(b) represent the Brillouin zone in the (110) (or equivalent) plane. Yet, as seen from those figures, the shapes of the corresponding Fermi surfaces are completely different. This directly shows the orientational tuning of the Fermi surface due to different confinement directions.

Figure 3(c) shows the energy-momentum map at the Γ point along the $\langle \bar{1}\,\bar{1}\,2\rangle$ direction, corresponding to the major axis of the ellipsoids forming the six-pointed-star Fermi surface. The dispersions of one light band and one heavy band are clearly visible. These constitute the ground state of the 2DEG. Additional subbands are not observed, implying that the band bending at the surface is too low to populate the upper quantum-well states. Within our resolution, the heavy and light bands are degenerate at Γ, with their band bottom located at about −57 meV. We fit simultaneously these dispersions and the whole Fermi surface of Fig. 3(a) using a simple tight-binding model [22]. The fit, shown by the continuous blue lines, yields Fermi momenta of about 0.07 and 0.36 Å^{-1} for, respectively, the light and heavy bands along $\langle \bar{1}\,\bar{1}\,2\rangle$. This gives an electron concentration $n_{2D}^{(111)} \approx 1.0 \times 10^{14}$ cm^{-2}, and effective masses listed in the third row of Table I.

We now draw some comparisons between the effective masses and thicknesses of the 2DEGs at the $SrTiO_3$ (001), (110), and (111) surfaces. Table I shows that, while the masses along the "natural" electron-hopping directions in the bulk ([001] and equivalent) are comparable between the 2DEGs at the $SrTiO_3$ (001) and (110) surfaces, the masses along [110] at the (110) surface, and all the masses of the 2DEG at the (111) surface, are very different from the ones expected from the tight-binding parameters describing the bulk or the 2DEG at the (001) surface. In this respect, note that if the confinement direction is [110] or [111], then the electrons moving in the 2DEG plane along a direction other than [001] will experience the confining potential gradient and the modified crystal field outside the surface, as they will hop in staircase patterns between first neighbors along [001] (or equivalent) directions—see Figs. 1(a)–1(d) and Refs. [8,19]. The understanding of these mass differences, also reported in quantum-well states at thin films of simple metals [27] or strongly correlated oxides [28], should be the subject of further theoretical works.

The maximal spatial extension d_{max} of the 2DEGs at the $SrTiO_3$ (110) and (111) surfaces can be estimated using a triangular potential well model [22]. We obtain $d_{max}^{110} \approx 1.7$ nm, which amounts to six two-dimensional layers or three bulk unit cells along [110], and $d_{max}^{111} \approx 1.9$ nm, corresponding to approximately nine layers of Ti (111), or again about three bulk unit cells along [111].

Finally, we note that the orbital ordering of the electronic states at the (110) and (111) surfaces of $SrTiO_3$ is different from the orbital ordering at the (100) surface. In the first two cases, the bands are degenerate within our experimental resolution, whereas at the (001) surface the smallest observed splitting between bands of different orbital character is of 50 meV [14]. As the confinement energy of each band is inversely proportional to its effective mass along the confinement direction [14], different surface orientations result in different orbital ordering. But along the [111] direction the effective masses of the three t_{2g} bands are identical, and so their degeneracy at the Γ point is not lifted by the confinement. Similarly, the effective masses of bands of different orbital character along [110] are quite similar (see Table I). Hence, the degeneracy lift is rather small and cannot be observed in our data. This demonstrates the influence of the confinement direction on the orbital ordering.

Several scenarios have been proposed to explain the origin of the 2DEG at the $LaAlO_3/SrTiO_3(001)$ interface. According to one scenario, the formation of a conducting sheet prevents the occurrence of a polar catastrophe in the material. Yet, the discovery of a confined 2DEG at the (001) surface of $SrTiO_3$, with characteristics similar to those of the above heterostructure, suggests that the driving mechanism may not be unique, as in the bare $SrTiO_3$ all the layers are electrically neutral. Instead, in the latter case, surface oxygen vacancies are believed to cause and to confine the gas [14,15,24]. Additionally, for the (110) and (111) $SrTiO_3$ surfaces, of nominal polar charge $4e$, one would expect a much larger carrier concentration in the 2DEG, and a very strong electric field confining the electrons in a narrow sheet at the surface. However, we observe that the carrier concentrations and thicknesses of the 2DEGs are quite comparable for all three orientations (this work and Ref. [14]): $n_{2D} \sim 10^{14}$ cm^{-2}, $d_{max} \sim 2$ nm. In fact, in the polar $SrTiO_3$ surfaces studied here, the polar catastrophe does not seem to be compensated by the electrons of the 2DEG, but by surface reconstructions or relaxations, while the 2DEG lies in the subsurface layers. Thus, although the 2D electronic structure (effective masses, orbital ordering) depends on the surface orientation, the thickness and carrier concentration of the 2DEG might be controlled by another factor, probably oxygen vacancies and/or lattice distortions induced by the synchrotron light irradiation, as discussed in the Supplemental Material [22].

In conclusion, our results show that the symmetries, electronic structure, and orbital ordering of the confined states at the surface of TMOs can be tailored by confining the electrons along different directions in the *same* material. Such orientational tuning echoes the differences of transport properties reported recently in $LaAlO_3/SrTiO_3$ (110)

and (111) interfaces [7–9]. In particular, from our data, the highly anisotropic transport behavior observed in the (110) interfaces [8] can be directly related to the twofold symmetry of the Fermi surface measured by ARPES. More generally, our results provide an exciting route for obtaining new types of 2D electronic states in correlated-electron oxides.

We thank V. Pillard for her contribution to the sample preparation. T. C. R. acknowledges funding from the RTRA Triangle de la Physique (Project No. PEGASOS). A. F. S.-S. and M. G. acknowledge support from the Institut Universitaire de France. This work is supported by public grants from the French National Research Agency (ANR) (Project LACUNES No. ANR-13-BS04-0006-01) and the "Laboratoire d'Excellence Physique Atomes Lumière Matière" (LabEx PALM Project ELECTROX) overseen by the ANR as part of the "Investissements d'Avenir" program (reference: ANR-10-LABX-0039).

[1] H. Takagi and H. Y. Hwang, An emergent change of phase for electronics, Science **327**, 1601 (2010).

[2] J. Mannhart and D. G. Schlom, Oxide interfaces—An opportunity for electronics, Science **327**, 1607 (2010).

[3] S. Thiel, G. Hammerl, A. Schmehl, C. W. Schneider, and J. Mannhart, Tunable quasi-two-dimensional electron gases in oxide heterostructures, Science **313**, 1942 (2006).

[4] A. D. Caviglia *et al.*, Electric field control of the $LaAlO_3/SrTiO_3$ interface ground state, Nature (London) **456**, 624 (2008).

[5] A. Brinkman *et al.*, Magnetic effects at the interface between non-magnetic oxides, Nat. Mater. **6**, 493 (2007).

[6] M. Salluzzo *et al.*, Structural and electronic reconstructions at the $LaAlO_3/SrTiO_3$ interface, Adv. Mater. **25**, 2333 (2013).

[7] G. Herranz, F. Sánchez, N. Dix, M. Scigaj, and J. Fontcuberta, High mobility conduction at (110) and (111) $LaAlO_3/SrTiO_3$ interfaces, Sci. Rep. **2**, 758 (2012).

[8] A. Annadi *et al.*, Anisotropic two-dimensional electron gas at the $LaAlO_3/SrTiO_3$ (110) interface, Nat. Commun. **4**, 1838 (2013).

[9] G. Herranz, N. Bergeal, J. Lesueur, M. Scigaj, N. Dix, and J. Fontcuberta, Orientational tuning of the 2D-superconductivity in $LaAlO_3/SrTiO_3$ interfaces, arXiv: 1305.2411.

[10] D. Xiao, W. Zhu, Y. Ran, N. Nagaosa, and S. Okamoto, Interface engineering of quantum Hall effects in digital transition metal oxide heterostructures, Nat. Commun. **2**, 596 (2011).

[11] K.-Y. Yang, W. Zhu, D. Xiao, S. Okamoto, Z. Wang, and Y. Ran, Possible interaction-driven topological phases in (111) bilayers of $LaNiO_3$, Phys. Rev. B **84**, 201104 (2011).

[12] A. Rüegg and G. A. Fiete, Topological insulators from complex orbital order in transition-metal oxides heterostructures, Phys. Rev. B **84**, 201103 (2011).

[13] D. Doennig, W. E. Pickett, and R. Pentcheva, Massive symmetry breaking in $LaAlO_3/SrTiO_3(111)$ Quantum wells: A three-orbital strongly correlated generalization of graphene, Phys. Rev. Lett. **111**, 126804 (2013).

[14] A. F. Santander-Syro *et al.*, Two-dimensional electron gas with universal subbands at the surface of $SrTiO_3$, Nature (London) **469**, 189 (2011).

[15] W. Meevasana, P. D. C. King, R. H. He, S.-K. Mo, M. Hashimoto, A. Tamai, P. Songsiriritthigul, F. Baumberger, and Z.-X. Shen, Creation and control of a two-dimensional electron liquid at the bare $SrTiO_3$ surface, Nat. Mater. **10**, 114 (2011).

[16] N. C. Plumb *et al.*, Mixed dimensionality of confined conducting electrons tied to ferroelectric surface distortion on an oxide, arXiv:1302.0708.

[17] P. D. C. King *et al.*, Subband structure of a two-dimensional electron gas formed at the polar surface of the strong spin-orbit perovskite $KTaO_3$, Phys. Rev. Lett. **108**, 117602 (2012).

[18] A. F. Santander-Syro *et al.*, Orbital symmetry reconstruction and strong mass renormalization in the two-dimensional electron gas at the surface of $KTaO_3$, Phys. Rev. B **86**, 121107 (2012).

[19] C. Bareille *et al.*, Two-dimensional electron gas with six-fold symmetry at the (111) surface of $KTaO_3$, Sci. Rep. **4**, 3586 (2014).

[20] A. Biswas *et al.*, Universal Ti-rich termination of atomically flat $SrTiO_3$ (001), (110), and (111) surfaces, Appl. Phys. Lett. **98**, 051904 (2011).

[21] J. Chang, Y.-S. Park, and S.-K. Kim, Atomically flat single-terminated $SrTiO_3$ (111) surface, Appl. Phys. Lett. **92**, 152910 (2008).

[22] See Supplemental Material at http://link.aps.org/supplemental/10.1103/PhysRevApplied.1.051002 for more details on the sample preparation, photon energy dependent matrix elements, the Fermi surface of $SrTiO_3(110)$, spatial extensions of the 2DEGs, and the UV dose dependence of the photoemission spectra.

[23] G. Khalsa and A. H. MacDonald, Theory of the $SrTiO_3$ surface state two-dimensional electron gas, Phys. Rev. B **86**, 125121 (2012).

[24] Z. Wang *et al.*, Anisotropic two-dimensional electron gas at $SrTiO_3(110)$, Proc. Natl. Acad. Sci. U.S.A. **111**, 3933 (2014).

[25] A. Mugarza, J. Ortega, A. Mascaraque, E. Michel, K. Altmann, and F. Himpsel, Periodicity and thickness effects in the cross section of quantum well states, Phys. Rev. B **62**, 12672 (2000).

[26] E. D. Hansen, T. Miller, and T. C. Chiang, Quantum-well or bulklike behaviour of Cu layers on Co, J. Phys. Condens. Matter **9**, L435 (1997).

[27] Y. Z. Wu, C. Y. Won, E. Rotenberg, H. W. Zhao, F. Toyoma, N. V. Smith, and Z. Q. Qiu, Dispersion of quantum well states in Cu/Co/Cu(001), Phys. Rev. B **66**, 245418 (2002).

[28] K. Yoshimatsu, K. Horiba, H. Kumigashira, T. Yoshida, A. Fujimori, and M. Oshima, Metallic quantum well states in artificial structures of strongly correlated oxide, Science **333**, 319 (2011).